Electrochemistry at the edge of a van der Waals heterostructure

Aleksandra Plačkić[1,2#], Tilmann J. Neubert[3#], Kishan Patel[1], Michel Kuhl[3], Kenji Watanabe[4], Takashi Taniguchi[4], Amaia Zurutuza[5], Roman Sordan[1*] and Kannan Balasubramanian[3*]

[1]L-NESS, Department of Physics, Politecnico di Milano, Via Anzani 42, 22100 Como, Italy

[2]BioSense Institute, University of Novi Sad, Dr Zorana Đinđića 1, 21000 Novi Sad, Serbia

[3]School of Analytical Sciences Adlershof (SALSA), IRIS Adlershof & Department of Chemistry, Humboldt-Universität zu Berlin, Unter den Linden 6, 10099 Berlin, Germany

[4]National Institute for Materials Science, 1-1 Namiki, 305-0044 Tsukuba, Japan

[5]Graphenea, Avenida de Tolosa 76, 20018 Donostia/San Sebastián, Spain

[#]*equal contribution*

**Corresponding author e-mail: roman.sordan@polimi.it & nano.anchem@hu-berlin.de*

ABSTRACT

Artificial van der Waals heterostructures, obtained by stacking layered two-dimensional materials, represent a novel material platform for investigating physicochemical phenomena and applications. Here, the electrochemistry at the one-dimensional edge of a graphene sheet, which is sandwiched between two hexagonal boron nitride (hBN) multilayer flakes, is reported. When such an hBN/graphene/hBN heterostructure is immersed in a solution, the basal plane of graphene is protected and isolated by the hBN stack, and the edge of the graphene sheet is exclusively available in the solution. This forms an electrochemical nanoelectrode, which enabled the investigation of electron transfer using several redox probes, e.g., ferrocene(di)methanol, hexaammineruthenium, methylene blue, dopamine and ferrocyanide. The relatively low capacitance of the van der Waals edge electrode facilitates cyclic voltammetry at very high scan rates (up to 1000 V/s). Using fast scan cyclic voltammetry imaging, redox species could be detected voltammetrically down to micromolar concentrations

with sub-second time resolution at the sandwiched graphene edge, promoted by the rapid equilibration of analyte species in the diffusion layer. Furthermore, the nanoband nature of the edge electrode allows its operation directly in water in the absence of added electrolyte. Finally, two adjacent edge electrodes could be realized in a redox-cycling format. In all, the van der Waals edge electrode is unique among nanoelectrodes as it enables investigations of all the above-mentioned phenomena in the same device. Due to its versatility, it constitutes a new avenue for nanoscale electrochemistry, which will be useful for studying electron transfer mechanisms as well as for the detection of analyte species in ultralow sample volumes.

INTRODUCTION

Heterostructures assembled using single sheets of two-dimensional (2D) materials are highly promising due to the novel properties they exhibit and several advantages they offer in comparison to their isolated counterparts.[1-3] Graphene has been widely explored as a building block in such heterostructures. As a one-atom thick material, the properties of graphene are highly sensitive to its environment. Especially the substrate, on which graphene is placed, dictates not only the physical properties but also the chemistry, such as reactivity and electron transfer (ET) properties.[4-6] By assembling a graphene sheet on an insulating 2D material such as hexagonal boron nitride (hBN), it is possible to decouple graphene from the underlying substrate, which renders graphene with properties close to that of free-standing graphene.[7] The lattice constant of hBN is similar to that of graphene, limiting the stress that can develop when graphene is placed or grown on such a crystal.[8] As the defect density in an hBN crystallite is orders of magnitude lower than in typical substrates such as silicon dioxide or glass, the intrinsic electronic properties of graphene can be directly exploited to realize devices showing superior electronic performance, such as high charge carrier mobility.[7] In an analogous manner, the environment to which graphene is exposed from the top has a significant effect on its physical properties. By using a van der Waals (vdW) heterostructure, wherein a graphene sheet is

encapsulated between two hBN layers, the sensitivity to the environment can be minimized thereby providing devices with high stability and improved electronic performance. This strategy has been exploited to realize high mobility electronic devices, high frequency and optical devices, memristors etc.[9-15] In such an architecture, the graphene sheet is physically well-isolated from the environment and the substrate.

For studying chemistry and electrochemistry, an hBN/graphene/hBN vdW heterostructure provides new prospects, whose exploration is still in its infancy.[16-17] It is a suitable platform to study electrochemical intercalation in stacked 2D materials.[15] In place of hBN, oxide layers could be used to realize graphene edges. By realizing pores in a graphene layer sandwiched between two Al_2O_3 layers, ionic transport through the pore could be measured.[18] However, ET with redox active species at the edge has not been investigated in that study. By contrast, the presence of hBN on both sides of graphene provides, in addition to an electronic isolation, also a clear chemical isolation of the basal plane of graphene from the environment,[4] opening up the possibility to study reactions exclusively at the edge, virtually free of substrate and basal plane effects. Electrochemistry at the graphene edge has been investigated using other fabrication strategies earlier.[19-23] With these edge electrodes, exclusive electrochemical modification of the edge has also been demonstrated.[20, 22] Furthermore, due to the unique format of the edge electrodes, large current densities and high ET rates have been estimated, which are not possible to observe using more classical ultramicroelectrodes.[18, 21, 23] In all these cases, the graphene sheet was directly placed on a silicon dioxide surface. The use of a vdW heterostructure effectively decouples the basal plane of graphene from the underlying surface and the environment, preserves the favorable properties of its basal plane, and allows electrochemical investigation exclusively of its edge in a decoupled environment.

There are specific advantages of studying electrochemistry at clean single graphene edges. Geometrically, the nanoscale size of the electrode opens the possibility of enhanced mass transport. [23-24] This is fundamentally important for studying fast electron transfer kinetics

(typically > 1 cm/s). [25] On the other hand, the edge poses a different electronic structure in comparison to the basal plane. Hence, improved electrochemical activity and catalytic effects are expected. [26-28] A graphene edge is a one-dimensional system and functions like a nanoband electrode. [19, 29] Often such micro-/nano-band electrodes are realized using metals, e.g., Au or Pt. [30] The use of carbon as a nanoelectrode opens an avenue for the study of selected redox active species, e.g., nicotinamide adenine dinucleotide (NADH), whose ET rates are known to be higher on carbon than on metals. [23, 31] A single carbon nanotube is a suitable candidate for a carbon-based linear nanoelectrode (two dimensions < 10 nm). [32] The current collection is however only at the ends of the nanotube, which may pose some limitations, e.g., due to scattering of electron transport along the nanotube. [33] By contrast, at a graphene edge, the current can be collected in parallel across the entire graphene edge. Hence, we can mainly readout signals due to ET free of scattering, which is further minimized when the sheet is embedded in the vdW heterostructure.

With this motivation, we present here the realization of one-dimensional (1D) graphene edge electrodes with a length of few microns sandwiched between two hBN multilayer sheets, where only the edge of graphene is in contact with the solution. Exploiting the unique properties of such an electrode, e.g., the small electrode area and high interfacial resistance, we demonstrate that we can perform electrochemistry at fast scan rates and work in water, free of added supporting electrolyte. Finally, we also show that these electrodes can be realized in a redox-cycling format, wherein redox active species reduced or oxidized at one electrode can be shuttled for ET to a second edge electrode in its close vicinity.

RESULTS AND DISCUSSION

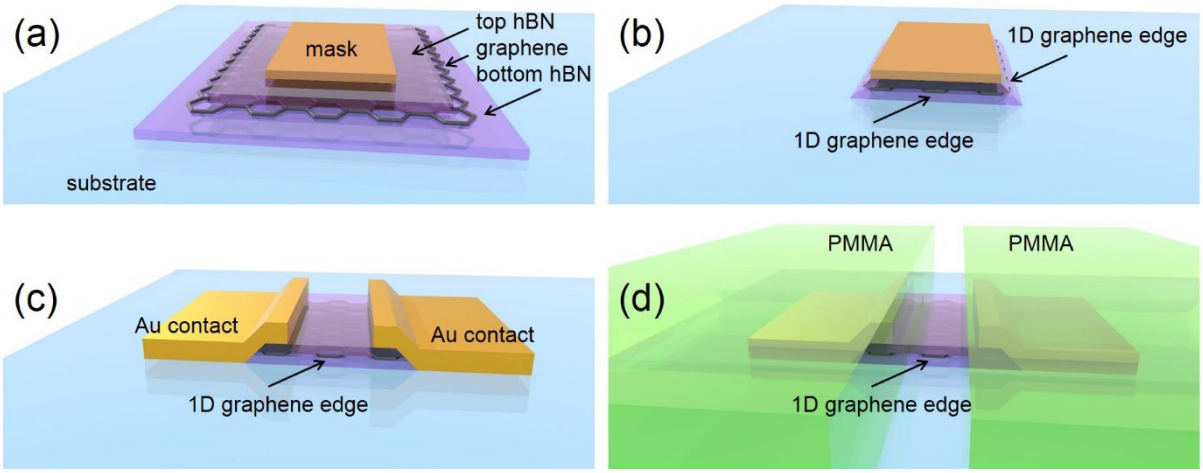

Figure 1. Simplified workflow showing the fabrication of a vdWEdge device. (a) An Al hard mask was fabricated on top of the hBN/graphene/hBN stack, which was assembled on top of a SiO_2/Si substrate by a hot pick-up technique.[34] (b) After RIE, the part of the stack unprotected by the mask was etched away. (c) After removal of the mask, the Au electrodes were fabricated on the opposite sides of the stack forming contacts to the exposed 1D edges of graphene. (d) The contacts were passivated by a PMMA layer such that the remaining 1D edges of graphene were exposed to the environment.

Figure 1 shows the fabrication steps and the layout of a typical van der Waals edge (vdWEdge) electrode, which comprises a monolayer graphene sheet sandwiched between two hBN multilayer flakes and contacted on two ends by Au electrodes. Complete details of the fabrication are given in the Methods section based on our previous work.[14, 35] In short, the fabrication of such a device started with the assembly of an hBN/graphene/hBN stack onto a SiO_2/Si substrate using a hot pick-up technique (Figure 1(a)).[34] The 1D edges of graphene were exposed on all four sides of the stack, after the stack was shaped in rectangular form by reactive-ion etching (RIE) using a hard mask (Figure 1(b)). Two sides of the stack were metallized to contact graphene along its 1D edges, while the other two sides were left uncovered to expose the 1D edges of graphene to the environment (Figure 1(c)). Electrical measurements were performed to confirm the formation of ohmic contacts to graphene. The mean resistance was 2.44 kΩ (19 devices) with a standard deviation of 0.75 kΩ for a graphene channel with a width of 10 μm and length of 4 μm. Finally, the electrodes were passivated using poly(methylmethacrylate) (PMMA).

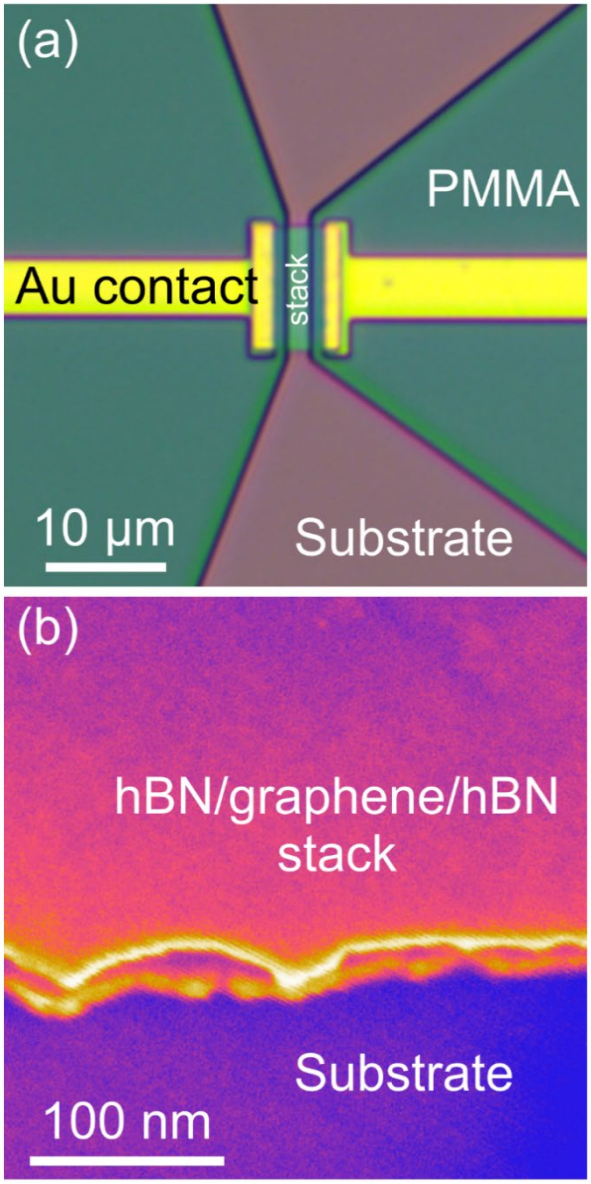

Figure 2. Different views of a vdWEdge device. (a) Optical image of a typical device in top-view with the hBN/graphene/hBN stack in between the Au contacts as indicated. (b) False-color high-resolution SEM image of the peripheral region of a vdWEdge device, where the two hBN crystals are discernible. The graphene edge lies open in between the edges of these two layers highlighted in yellow.

An optical image of the final device showing the top-view, identifying the different parts, is shown in Figure 2(a). Figure 2(b) shows a close-up scanning electron microscope (SEM) image of the edge of the assembled stack, where the top and bottom hBN layers are clearly distinguishable, confirming that the basal plane of graphene is well protected. Further optical and atomic force microscopy (AFM) images of a device with another layout are shown in Supporting Information (SI) Figure S1.

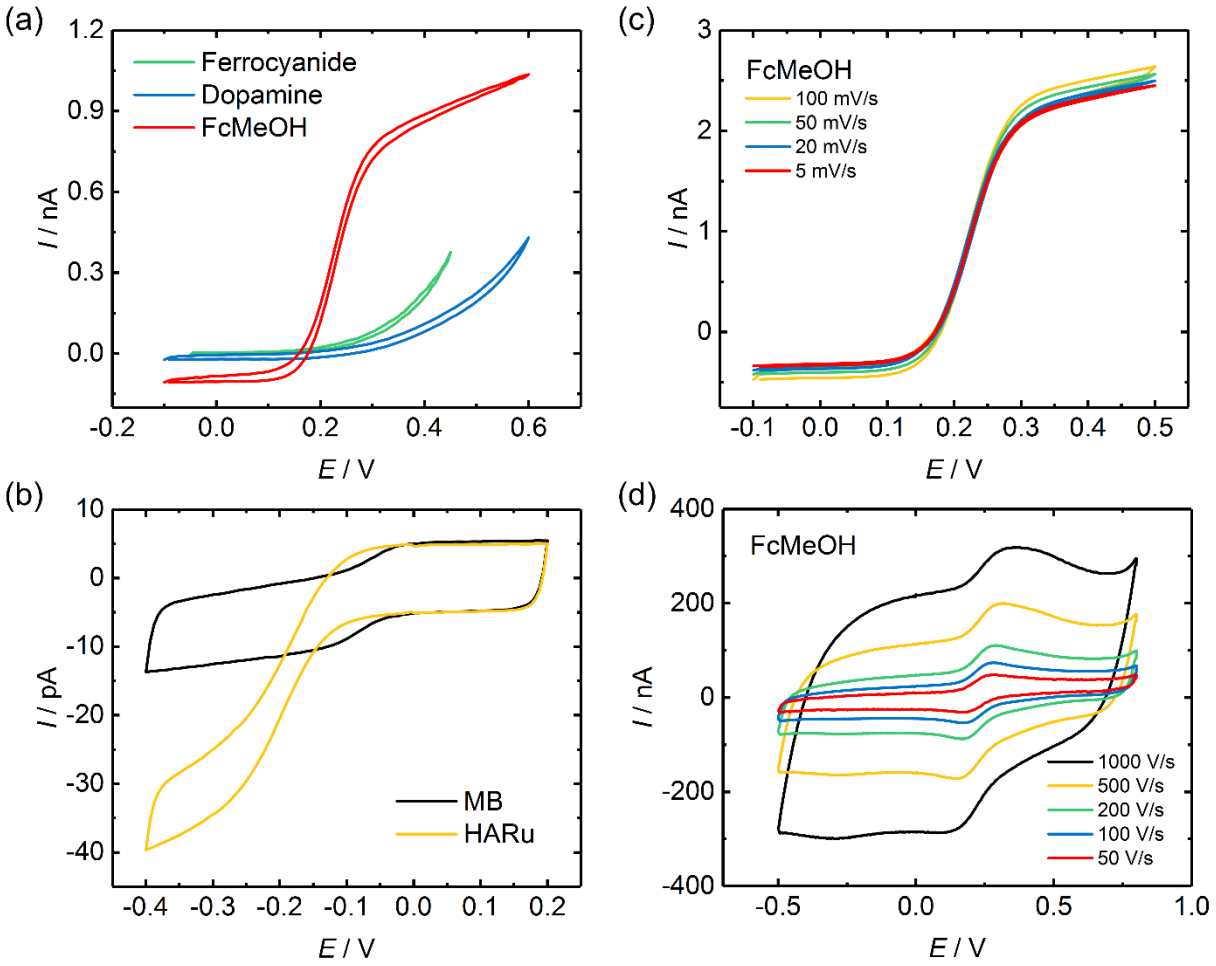

Figure 3. CVs of selected redox-active species at vdWEdge electrodes. (a) CVs of species undergoing oxidation: ferrocyanide (0.1 mM), dopamine (1 mM), ferrocenemethanol – FcMeOH (1 mM). (b) CVs of molecules undergoing reduction: methylene blue – MB (0.1 mM), hexaammineruthenium – HARu (0.1 mM). (c,d) CVs at varying scan rates for the oxidation of FcMeOH (1 mM slow scan, 5 mM fast scan) at a vdWEdge electrode – low scan rates (c) and high scan rates (d). The potentials are measured with reference to a commercial Ag/AgCl (3M KCl) reference electrode. Scan rate was 100 mV/s in (a) and (b). For dopamine and FcMeOH, a phosphate buffer (pH 6.7, 100 mM ionic strength) was used. The other measurements were performed in 0.1 M KCl.

We first evaluate ET with classical redox-active species at the vdWEdge as shown in the cyclic voltammograms (CVs) in Figure 3. Figure 3(a) shows the oxidation of ferrocyanide (FeCN), dopamine (DA) and ferrocenemethanol (FcMeOH), while Figure 3(b) shows the reduction of hexaammineruthenium and methylene blue at a vdWEdge electrode at low scan rates. Except for DA and FeCN, the CVs show nearly a sigmoidal shape, signifying a quasi-steady-state response, typical for one-dimensional nanoelectrodes.[23, 30, 36] Figure 3(c) presents CVs of FcMeOH with varying scan rate (rates < 100 mV/s), where it is apparent that the Faradaic response is independent of the scan rate. Only the capacitive current increases. These

observations confirm that we indeed measured the response at the edge working as a nanoelectrode.[23, 30]

Due to the miniscule size (typically 2 µm length at an estimated height of approximately 1 nm) of the vdWEdge electrode, the mass transport rate is extremely high. Hence using such electrodes, we have the capability to measure a broad range of ET rates with redox active species.[25, 30] The non-sigmoidal nature of the CV with DA and FeCN suggests that ET for these two cases is kinetically limited and is relatively slow in comparison to FcMeOH at the vdWEdge. Both $FeCN^6$ and DA[37] are known to act as inner sphere probes on carbon surfaces and are hence sensitive to the surface morphology, defects, the proportion of edges, and the chemical composition of the terminal functional groups. The comparatively lower ET rate with FeCN is consistent with previous observations on mm-long graphene edge electrodes.[23] A relatively slow ET with DA at the vdWEdge indicates that the chemical composition of our edge is most likely different from other graphitic or carbon electrodes.[26, 38-41] In previous work on ET with DA at carbon electrodes, often a quasi-reversible CV has been reported.[40] In contrast, we were only able to observe an oxidation wave with DA. Even on the basal plane of our graphene electrodes, ET with DA appears to be quite inefficient (see Figure S2 in SI). We attribute the sluggish ET kinetics with DA to the absence of deliberately introduced functional groups either at the edge or at the basal plane of the graphene sheet.[42] Moreover, the plasma conditions we use (e.g., SF_6 plasma for shaping the edge) may render the edge with a chemistry that does not allow for a fast electron transfer with DA. In the future, we plan to mitigate this through appropriate (electro)chemical modification of the edge.

In contrast to previously reported mm-long edge electrodes,[19-20, 23] the electrode area in a vdWEdge electrode is smaller by at least two orders of magnitude and the currents were < 1 nA. Hence, a simpler two-electrode setup can be used avoiding the need for a third current-collecting counter electrode.[30, 43] Using our electrodes, we were able to detect redox active species down to micro molar concentrations (see Figure S3 in SI).

The small area of the vdWEdge nanoelectrode corresponds to a drastically low double layer capacitance, which is even lower than our system capacitance of 50 pF (see Figure S4 for details). Hence, using our current setup we cannot estimate the actual capacitance of the vdWEdge. The low capacitance can however be exploited to investigate ET at high scan rates. Figure 3(d) shows the obtained response for FcMeOH at a vdWEdge at high scan rates (50-1000 V/s). Although the capacitive current increases with scan rate, we are clearly able to observe the redox waves of FcMeOH. In contrast to the low scan rate CVs showing a quasi steady state response (Figure 3c), here we observed conventional peak-shaped voltammograms related to oxidation and reduction. Such a behavior is expected for a nanoelectrode. Assuming that the edge is exclusively in contact with the solution, the diffusion profile is expected to be hemi-cylindrical near the vdWEdge. This can be considered a variant of the quarter-cylinder diffusion profile reported for long graphene edge electrodes directly lying on a SiO_2 substrate.[23] For higher scan rates, the diffusion layer however becomes thinner and planar diffusion starts dominating mass transport.[36, 44] As a result, characteristic redox peaks appear at high scan rates. We do not expect to see any tunneling through the hBN layers, since we have an insulating hBN crystallite of several layers assembled tightly on and below the graphene sheet.[45] This is further justified by considering that multilayer hBN with a very high resistance constitutes a large energy barrier for electron tunneling[46] and hence blocks ET completely to redox active species in solution. What we cannot however completely exclude is the possibility that not just the atomic edge, but a certain width (< 5 nm) of the graphene sheet in the edge region encounters the solution. This could be thought of as a nanoscale flat-band electrode. However, we cannot confirm this only from the CVs. Nevertheless, the diffusion profile is expected to be convergent also in this case.[47-48]

We have exploited the ability to work at high scan rates to explore the use of fast-scan cyclic voltammetry (FSCV)[49-50] at our vdWEdge electrodes. FSCV has been widely used for the detection of redox-active species such as neurotransmitters, nucleobases and antioxidants.[43, 50-

[53] Due to the high time resolution achievable, it has found application for the detection of release of DA and other molecules in vivo in different biological species.[54-56] Furthermore, by an appropriate design of the voltage waveform, multiplex detection, ET mechanisms as well as improved detection of antioxidants have been demonstrated.[57-58] Performing FSCV in a two-electrode setup provides a further advantage of a simplified cell setup and compact instrumentation.

Figure 4 presents FSCV data obtained at a vdWEdge electrode for the detection of 0.5 mM ferrocenedimethanol (FDM) in a two-electrode setup. Figure 4(a) shows a map of the measured current (after background subtraction) starting in 0.1 M KCl and upon addition of FDM at time t = 4 s. A clear response for oxidation is seen at anodic potentials > 0.15 V. A time profile (cross-section across the map in Figure 4(a)) is shown in Figure 4(b), where it is apparent that we can detect the voltammetric response at the vdWEdge with sub-second resolution.

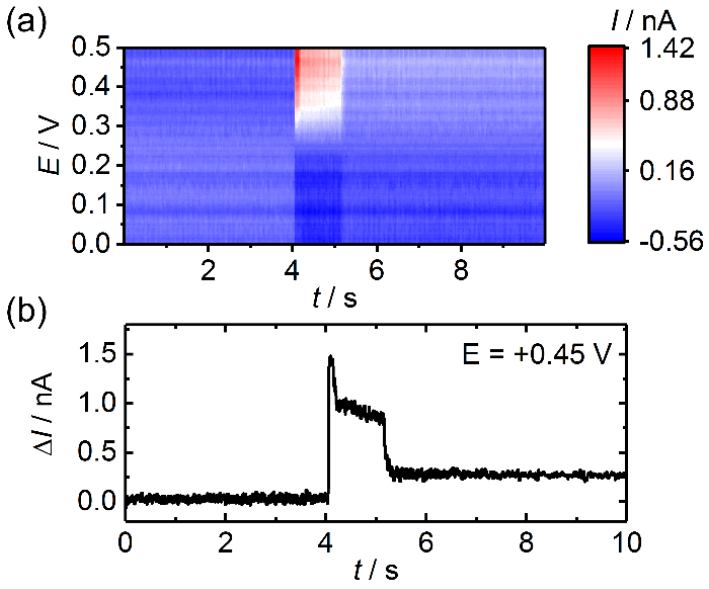

Figure 4. FSCV of FDM at a vdWEdge electrode. (a) A color map showing the voltammetric response during the entire measurement cycle. The measurement starts at t = 0 s with only 0.1 M KCl. At t = 4 s, FDM is injected to achieve a final concentration of 0.5 mM. The voltage is continuously scanned in the range of 0 to 0.5 V at a rate of 100 V/s during the entire measurement. Only the forward cycle is shown here. (b) A cross-section of the measured voltammetric response in (a), showing the evolution of current at a voltage of +0.45 V. The data are background subtracted using the current response in the first cycle. The potentials are with reference to an Ag/AgCl wire reference electrode.

Moreover, there is an increase in current after the addition of FDM, which shows an initial slow relaxation followed by a faster relaxation to approach a final steady state with a constant current. This indicates that a stable diffusion layer is set up very fast (in less than a second) and there is a constant rate of oxidation afterward.[30] Since we need just a two-electrode setup, such measurements can be carried out even in a very small droplet, enabling detection in ultra-low sample amounts. For the data in Figure 4, the analyte volume was 5 µL and an analyte amount of just 2.5 nanomoles. By appropriate miniaturization of the reference electrode, we believe that it would be possible to reduce this amount further by at least an order of magnitude. Figure S5 in SI shows another example of FSCV at a smaller concentration of 10 µM. For concentrations much lower than this value, the signals were buried in noise. This can be understood by considering that the miniscule electrode area sets a lower limit of current that can be measured free of noise. Hence the detection limit is in the micromolar range and is somewhat higher than substrate-supported graphene edge.[23] Nevertheless, the low capacitance and the small footprint give a clear advantage of very fast measurement as well as rapid equilibration of the diffusion layer.

There are some differences to previously reported FSCV work.[50-51] The most widely used analyte is DA,[52] the detection of which often requires adsorption on the electrode, which is typically enabled by using a hold potential between two consecutive CV cycles in an FSCV experiment.[38] Other analytes could be detected either via adsorption or by diffusion.[59-60] At our electrodes, we were not able to observe an adsorption-based response systematically. In cases where there was an indication of adsorption, the electrode was increasingly blocked irreversibly with every measurement cycle. This could most likely be mitigated in the future by performing appropriate chemical modification[55] of the edge.

Another important aspect of a vdWEdge is that the interfacial resistance, when operating in liquids, is quite high,[43] since only a small electrode region encounters the solution. Hence, it is interesting to look at the possibility of working in electrolyte-free media.[61] Already several

decades ago, it was proposed and shown that nanoelectrodes with sub-micron dimensions are suitable for the study of redox species in solutions free of supporting electrolyte.[62] A two-electrode configuration is more advantageous, since it reduces noise and allows for a simple setup.[62-64]

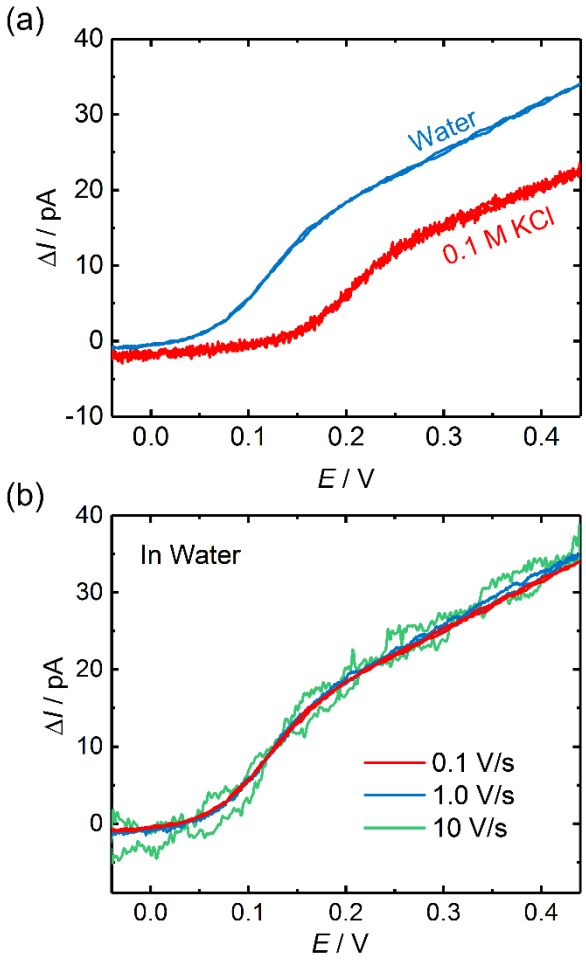

Figure 5. Electrochemistry of 100 µM FDM in water free of supporting electrolyte. (a) Comparison of background-subtracted CV measured at a scan rate of 0.1 V/s without added supporting electrolyte (blue curve) to that measured with added 0.1 M KCl (red curve). (b) CVs measured at varying scan rates without added supporting electrolyte. The potentials are with reference to an Ag/AgCl wire reference electrode.

Figure 5(a) compares typical background-subtracted two-electrode CVs of FDM in water measured at the same vdWEdge electrode at 0.1 V/s in 0.1 M KCl (red curve) and without any added supporting electrolyte (blue curve). The CV in water shows a slightly higher current and an apparent cathodic shift in the electrochemical response. Otherwise, the two curves are similar. The higher quasi-steady state current can be explained by a reduction in resistance after

oxidation of the neutral FDM species to a positively charged ion, which accumulates/diffuses at the vdWEdge-electrolyte interface and decreases the resistance.[65-68]

Nearly no hysteresis was observed in the background-subtracted CVs during the forward and backward scans, suggesting that we are able to obtain a stable quasi-steady-state response even in the absence of added electrolyte. Although we do not deliberately add any supporting electrolyte, trace amounts of ionic species cannot be avoided,[69] which enabled the observation of a quasi-sigmoidal ET response.[70] We attribute the shift in the CV along the potential scale to a shift in the electrode potential of the reference electrode. A chloride coated silver wire served as combined reference and counter electrode for both measurements. For the measurement in water, there was no added chloride. Hence, the chloride concentration is determined by the equilibrium between the AgCl coating on the silver wire and residual chloride ions in solution, as determined by the low solubility product of AgCl. The electrode potential of the Ag/AgCl wire in such a situation is lower (cathodic offset) than the potential when 0.1 M KCl is present in the solution.

In previous studies at ultramicroelectrodes, a shift in the half-wave potential has been predicted and observed for the oxidation of ferrocene when the supporting electrolyte concentration is reduced.[70-71] The shift was however anodic, which is not what we observed here. Another alternative explanation for the potential shift could be an iR drop (parasitic voltage drop due to uncompensated solution resistance), due to a difference in resistance with and without electrolyte, caused by changes in ionic composition in the diffusion layer as a result of the redox reaction.[61, 72] However, in such a situation, a significant distortion of the entire CV would be expected, which we did not observe in our CVs (see Figure S6 in SI). This kind of distortion has, however, mainly been reported in solvents of low dielectric strength.[73] Most likely, it appears that the iR drop is minimized due to the ultra-small interfacial area and pA currents. With a solution resistance in the MΩ range, the ohmic drop is significantly below 1 mV. Figure 5(b) presents background-subtracted CVs at three different scan rates measured in water, where

it is apparent that the quasi steady state response is preserved without any shift in potential or distortion in the CV or increase in hysteresis even up to a scan rate of 10 V/s. From these data, it is clear that our vdWEdge electrodes can reliably be used in solutions without added electrolyte.

The vdWEdge electrode constitutes a nanoelectrode, two of which can be assembled facing each other in a straightforward manner using our fabrication methodology. The availability of two such nanoelectrodes in close vicinity opens an avenue for specialized electrochemical experiments such as redox cycling.[74-75] Here one electrode serves as a generator where a redox species is oxidized, while the generated oxidized species is reduced at the other. This allows for a positive feedback using which the redox species shuttles between the two electrodes leading to an amplification of the current. [76] Moreover, such an assembly can be used for studying mechanisms of redox kinetics, electrochemiluminescence and titrations.[77-79]

We have evaluated the capability of redox cycling, by realizing two vdWEdge electrodes facing each other, with an open nanochannel in between, as illustrated by the schematic in Figure 6(a), an optical image in Figure 6(b) and an SEM image in Figure 6(c). We have also realized other layouts in interdigitated format (see another example in Figure S7 in SI). However, the current responses were qualitatively similar in all electrodes. Figure 6(d) shows typical background-subtracted current response for 0.6 mM FDM (in 0.1 M KCl) in generator-collector mode at a redox cycling vdWEdge gap. Such a measurement was carried out by biasing the two vdWEdge electrodes with respect to a chloridified Ag wire as the counter/reference electrode (see Methods section for details). While the collector electrode was maintained at a constant potential of -0.05 V, the generator potential was scanned in the displayed potential range and the currents at both electrodes were measured. It is clear in Figure 6(d) that, at potentials > 0.15 V, the FDM molecules oxidized (red curve) by the generator electrode are reduced at the collector, which results in a cathodic current (blue curve). However, the current at the collector electrode is only 20% of the current observed at the generator electrode. We attribute this to the

rather large electrode spacing of 200 nm in comparison to the edge electrode dimension of a few nm.[74] Moreover, the convergent diffusion profile[23] leads to a rapid diffusion of the generated reduced species, explaining the low collection efficiency of around 20%. Nevertheless, the data confirm that the two electrodes are able to work in unison, through exchange of species from one electrode to the other. The collection efficiency could be improved by realizing closed nanochannels or having a smaller electrode spacing.

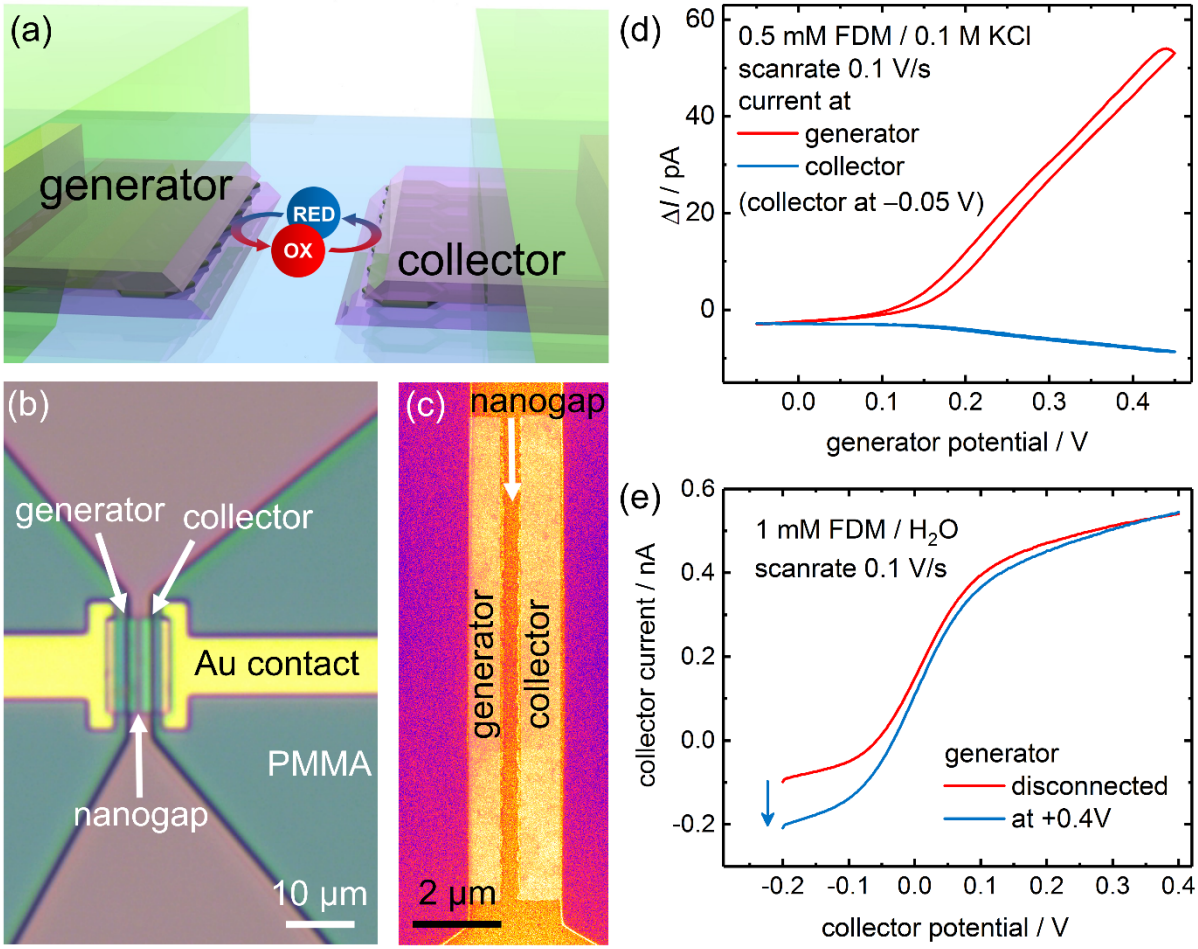

Figure 6. Redox cycling in a vdWEdge nanogap device. (a) Schematic of the dual vdWEdge electrode with a nanogap. The scheme shows one example of redox cycling where the collector electrode on the right is maintained at a constant cathodic potential, while the generator electrode potential is scanned in a selected voltage range where oxidation occurs. (b) Optical and (c) false-color SEM images showing top view of such a redox cycling vdWEdge electrode with a gap of 200 nm. (d) CVs obtained in 0.1 M KCl for the redox cycling of FDM with the collector electrode maintained at a potential of -0.05 V as exemplified in (a). (e) CVs obtained at the collector electrode in water (without added electrolyte) for the redox cycling of FDM with the generator electrode either disconnected or maintained at an anodic potential. The potentials are measured with reference to an Ag/AgCl wire reference electrode.

We also explored the possibility of redox cycling in supporting-electrolyte-free water as shown in Figure 6(e). The red curve shows the response obtained at the collector electrode without connecting the generator electrode, while the blue curve shows the response when the generator electrode was kept at a constant potential of +0.4 V. In the latter case, the generator produced reduced species, whose concentration increased locally, resulting in a higher current (indicated by the blue arrow) at the collector electrode. With this, we have demonstrated that using the vdWEdge electrode it is also possible to investigate redox cycling in media free of added electrolyte. In such electrodes, not only the diffusion layer but also the double layer of the two electrodes must overlap each other.[80] Future work will shed more light on the effect of this overlap. Furthermore, ion migration and electrostatic effects are expected to play an important role when using charged redox active species.[65]

CONCLUSION

In conclusion, we demonstrated the capability of performing electrochemistry at the 1D edge of a single graphene sheet sandwiched between two hBN crystallites. The unique geometry of the vdWEdge electrode and its small size opens up the possibility to study interfacial ET with several advantages. We showed that using such electrodes, FSCV could be deployed to study ET processes at very high scan rates with a very good time resolution. In this work, we have utilized FSCV in its simplest form. In the future, complex waveforms may be experimented for the detection of species via adsorption or for the sensing of multianalyte species.[57] We also described that it is possible to record CVs and perform redox cycling in water without added supporting electrolyte. Currently, the passivation layer on our devices is not well suited for experiments in organic solvents. For the future, more stable passivation layers can be utilized to enable this possibility. In such devices, the actual effect of iR drop can be more carefully investigated when working in organic solvents of lower dielectric constant.[73, 81] The ability to study ET in the absence of electrolyte may provide a platform for an unambiguous

understanding of ET mechanisms, free of diffusion and supporting electrolyte effects.[30, 82] Finally, chemical functionalization can be utilized to modulate ET at the vdWEdge, thereby expanding the spectrum of heterogeneous reactions that can be studied.

EXPERIMENTAL SECTION

Device fabrication. A hot pick-up technique[34] was used for the assembly of hBN/graphene/hBN vdW stacks. A glass slide with a polydimethylsiloxane block covered by polypropylene carbonate (PPC) was used to assemble the stacks. Due to the thermoplastic properties of PPC, hBN and graphene flakes were picked up from the initial substrate at 40 °C and subsequently released on the target substrate at 80-110 °C. The target substrate was highly resistive Si (resistivity of 5 kΩcm) with a 1-µm-thick SiO_2 layer on top. After the deposition, the heterostructures were baked for 5 minutes at 160 °C and cleaned in acetone for ~ 30 minutes. The thickness of the chosen hBN flakes was in the range of 25-40 nm to provide sufficient chemical and electrical isolation (e.g., to prevent electron tunneling through the flakes). The hBN flakes were exfoliated from synthetic hBN crystals, while both exfoliated graphene and graphene grown by chemical vapor deposition were used.
The stacks were patterned in two RIE steps using an Al mask. The masks were patterned on top of the stacks by electron-beam (e-beam) lithography (using Raith eLINE at 10-30 keV) and deposited by evaporating Al in an e-beam evaporator at a base pressure of ~ 10^{-6} mbar. In the first RIE step, only the top hBN flake was etched by SF_6 forming a rectangle (typically 11 µm × 8 µm) protected by a 40-nm-thick Al mask. The final device layout was defined in the second RIE step when the entire hBN/graphene/hBN stack was etched, exposing graphene edges. The hBN flakes were etched by SF_6 and graphene by O_2 plasma using an 80-nm-thick Al mask. The Al masks were removed after each RIE step by a mixture of tetramethylammonium hydroxide and H_2O.
The edge contacts to graphene were defined at the opposite sides of the stacks by e-beam lithography and e-beam evaporation of 80 nm of pure Au. The deposition of Au was followed by a lift-off process. Finally, the Au electrodes were passivated by a 200-nm-thick layer of PMMA to avoid their contact with the solution used in electrochemical measurements. A 2-µm-long opening in the passivation layer (between the contacts) was patterned by e-beam lithography to expose the edges of graphene to the environment.

Electrochemical instrumentation. Electrochemical measurements in a three-electrode configuration were performed using an Ivium Compactstat bipotentiostat with the vdwEdge as working electrode, a Pt wire as a counter electrode, and Ag/AgCl as reference electrode. The reference electrode was either a commercial DRIREF-450 (WPI Inc.) or a homemade chloridified Ag wire (50 µm diameter). The potential offset of the latter in 0.1 M KCl with respect to the commercial electrode was less than 50 mV. For the two-electrode configuration, two homemade setups were utilized, where the vdWEdge acted as the working and the Ag/AgCl wire as the counter electrode. In a first setup, we used a Vortis Controller of a Bruker JPK NanoTracker 4 system. Specifically a voltage source channel was used for applying the potential and an analog-to-digital converter (ADC) for measuring voltage input. The current passing through the electrochemical cell was amplified using an I/V-converter (Femto DLPCA-200) and the voltage was sampled by the ADC at a suitable frequency between 500 Hz and 20 kHz depending on the scan rate. In a second setup, a two-channel Keithley sourcemeter 2636B was used to measure currents by applying a desired voltage waveform. In this case, the devices

were placed in a FormFactor Summit 11000 probe station. For redox-cycling measurements, the currents from both electrodes were measured independently using the two channels. The Keithley sourcemeter was also used to measure the resistance of the encapsulated graphene between the two Au electrodes. All measurements were carried out in an appropriately shielded Faraday cage.

Surface characterization. Optical images were obtained on a Leica DM6 M, AFM images using a Bruker JPK Nanowizard 4 or a Veeco Innova, and SEM images using a Raith eLINE e-beam system.

ACKNOWLEDGEMENTS

This project was partly funded by the Deutsche Forschungsgemeinschaft (DFG, German Research Foundation) - 425219379; INST 276/754-1 and EU Horizon 2020 projects Graphene Flagship Core 3 (grant agreement ID 881603) and ANTARES (grant agreement ID 739570). Funding from the DFG as part of the excellence initiative *via* the Graduate School of Analytical Sciences Adlershof (GSC1013 SALSA) is gratefully acknowledged.

CONFLICT OF INTEREST

The authors declare no conflict of interest

DATA AVAILABILITY

The data that support the findings of this study are available from the corresponding author upon reasonable request.

REFERENCES

1. Geim, A. K.; Grigorieva, I. V., Van der Waals heterostructures. *Nature* **2013,** *499* (7459), 419-25.

2. Novoselov, K. S.; Mishchenko, A.; Carvalho, A.; Castro Neto, A. H., 2D materials and van der Waals heterostructures. *Science* **2016,** *353* (6298), aac9439.

3. Zhang, H., Ultrathin Two-Dimensional Nanomaterials. *ACS Nano* **2015,** *9* (10), 9451-69.

4. Wang, Q. H.; Jin, Z.; Kim, K. K.; Hilmer, A. J.; Paulus, G. L.; Shih, C. J.; Ham, M. H.; Sanchez-Yamagishi, J. D.; Watanabe, K.; Taniguchi, T.; Kong, J.; Jarillo-Herrero, P.; Strano, M. S., Understanding and controlling the substrate effect on graphene electron-transfer chemistry via reactivity imprint lithography. *Nat. Chem.* **2012,** *4* (9), 724-32.

5. Hui, J.; Zhou, X.; Bhargava, R.; Chinderle, A.; Zhang, J.; Rodríguez-López, J., Kinetic Modulation of Outer-Sphere Electron Transfer Reactions on Graphene Electrode with a Sub-surface Metal Substrate. *Electrochim. Acta* **2016,** *211*, 1016-1023.

6. Wehrhold, M.; Neubert, T. J.; Yadav, A.; Vondracek, M.; Iost, R. M.; Honolka, J.; Balasubramanian, K., pH sensitivity of interfacial electron transfer at a supported graphene monolayer. *Nanoscale* **2019,** *11* (31), 14742-14756.

7. Dean, C. R.; Young, A. F.; Meric, I.; Lee, C.; Wang, L.; Sorgenfrei, S.; Watanabe, K.; Taniguchi, T.; Kim, P.; Shepard, K. L.; Hone, J., Boron nitride substrates for high-quality graphene electronics. *Nat. Nanotechnol.* **2010,** *5* (10), 722-6.

8. Yang, W.; Chen, G.; Shi, Z.; Liu, C. C.; Zhang, L.; Xie, G.; Cheng, M.; Wang, D.; Yang, R.; Shi, D.; Watanabe, K.; Taniguchi, T.; Yao, Y.; Zhang, Y.; Zhang, G., Epitaxial growth of single-domain graphene on hexagonal boron nitride. *Nat. Mater.* **2013,** *12* (9), 792-7.

9. Mayorov, A. S.; Gorbachev, R. V.; Morozov, S. V.; Britnell, L.; Jalil, R.; Ponomarenko, L. A.; Blake, P.; Novoselov, K. S.; Watanabe, K.; Taniguchi, T.; Geim, A. K., Micrometer-scale ballistic transport in encapsulated graphene at room temperature. *Nano Lett.* **2011,** *11* (6), 2396-9.

10. Wang, L.; Meric, I.; Huang, P. Y.; Gao, Q.; Gao, Y.; Tran, H.; Taniguchi, T.; Watanabe, K.; Campos, L. M.; Muller, D. A.; Guo, J.; Kim, P.; Hone, J.; Shepard, K. L.; Dean, C. R., One-Dimensional Electrical Contact to a Two-Dimensional Material. *Science* **2013,** *342* (6158), 614-617.

11. Meric, I.; Dean, C. R.; Petrone, N.; Wang, L.; Hone, J.; Kim, P.; Shepard, K. L., Graphene Field-Effect Transistors Based on Boron–Nitride Dielectrics. *Proc. IEEE* **2013,** *101* (7), 1609-1619.

12. Kretinin, A. V.; Cao, Y.; Tu, J. S.; Yu, G. L.; Jalil, R.; Novoselov, K. S.; Haigh, S. J.; Gholinia, A.; Mishchenko, A.; Lozada, M.; Georgiou, T.; Woods, C. R.; Withers, F.; Blake, P.; Eda, G.; Wirsig, A.; Hucho, C.; Watanabe, K.; Taniguchi, T.; Geim, A. K.; Gorbachev, R. V., Electronic properties of graphene encapsulated with different two-dimensional atomic crystals. *Nano Lett.* **2014,** *14* (6), 3270-6.

13. Withers, F.; Del Pozo-Zamudio, O.; Mishchenko, A.; Rooney, A. P.; Gholinia, A.; Watanabe, K.; Taniguchi, T.; Haigh, S. J.; Geim, A. K.; Tartakovskii, A. I.; Novoselov, K. S., Light-emitting diodes by band-structure engineering in van der Waals heterostructures. *Nat. Mater.* **2015,** *14* (3), 301-6.

14. Caridad, J. M.; Calogero, G.; Pedrinazzi, P.; Santos, J. E.; Impellizzeri, A.; Gunst, T.; Booth, T. J.; Sordan, R.; Boggild, P.; Brandbyge, M., A Graphene-Edge Ferroelectric Molecular Switch. *Nano Lett.* **2018,** *18* (8), 4675-4683.

15. Zhao, S. Y. F.; Elbaz, G. A.; Bediako, D. K.; Yu, C.; Efetov, D. K.; Guo, Y.; Ravichandran, J.; Min, K. A.; Hong, S.; Taniguchi, T.; Watanabe, K.; Brus, L. E.; Roy, X.; Kim, P., Controlled Electrochemical Intercalation of Graphene/h-BN van der Waals Heterostructures. *Nano Lett.* **2018,** *18* (1), 460-466.

16. Velický, M.; Toth, P. S., From two-dimensional materials to their heterostructures: An electrochemist's perspective. *Appl. Mater. Today* **2017,** *8*, 68-103.

17. Velický, M.; Dryfe, R. A. W., Chapter 10 - Electrochemistry of 2D nanomaterials. In *Frontiers of Nanoscience*, Wain, A. J.; Dickinson, E. J. F., Eds. Elsevier: 2021; Vol. 18, pp 485-536.

18. Banerjee, S.; Shim, J.; Rivera, J.; Jin, X.; Estrada, D.; Solovyeva, V.; You, X.; Pak, J.; Pop, E.; Aluru, N.; Bashir, R., Electrochemistry at the edge of a single graphene layer in a nanopore. *ACS Nano* **2013,** *7* (1), 834-43.

19. Li, K.; Jiang, J.; Dong, Z.; Luo, H.; Qu, L., A linear graphene edge nanoelectrode. *Chem. Commun.* **2015,** *51* (42), 8765-8.

20. Bellunato, A.; Schneider, G. F., Electrophilic radical coupling at the edge of graphene. *Nanoscale* **2018,** *10* (25), 12011-12017.

21. Yuan, W.; Zhou, Y.; Li, Y.; Li, C.; Peng, H.; Zhang, J.; Liu, Z.; Dai, L.; Shi, G., The edge- and basal-plane-specific electrochemistry of a single-layer graphene sheet. *Sci. Rep.* **2013,** *3* (1), 2248.

22. Yadav, A.; Iost, R. M.; Neubert, T. J.; Baylan, S.; Schmid, T.; Balasubramanian, K., Selective electrochemical functionalization of the graphene edge. *Chem. Sci.* **2019,** *10* (3), 936-942.

23. Yadav, A.; Wehrhold, M.; Neubert, T. J.; Iost, R. M.; Balasubramanian, K., Fast Electron Transfer Kinetics at an Isolated Graphene Edge Nanoelectrode with and without Nanoparticles: Implications for Sensing Electroactive Species. *ACS Appl. Nano Mater.* **2020,** *3* (12), 11725-11735.

24. Godino, N.; Borrisé, X.; Muñoz, F. X.; del Campo, F. J.; Compton, R. G., Mass Transport to Nanoelectrode Arrays and Limitations of the Diffusion Domain Approach: Theory and Experiment. *The Journal of Physical Chemistry C* **2009,** *113* (25), 11119-11125.

25. Oja, S. M.; Wood, M.; Zhang, B., Nanoscale Electrochemistry. *Anal. Chem.* **2013,** *85* (2), 473-486.

26. Banks, C. E.; Davies, T. J.; Wildgoose, G. G.; Compton, R. G., Electrocatalysis at graphite and carbon nanotube modified electrodes: edge-plane sites and tube ends are the reactive sites. *Chem. Commun.* **2005,** (7), 829-41.

27. Kobayashi, Y.; Fukui, K.-i.; Enoki, T.; Kusakabe, K., Edge state on hydrogen-terminated graphite edges investigated by scanning tunneling microscopy. *Phys. Rev. B* **2006,** *73* (12), 125415.

28. Shen, A.; Zou, Y.; Wang, Q.; Dryfe, R. A.; Huang, X.; Dou, S.; Dai, L.; Wang, S., Oxygen reduction reaction in a droplet on graphite: direct evidence that the edge is more active than the basal plane. *Angew. Chem. Int. Ed. Engl.* **2014,** *53* (40), 10804-8.

29. Li, D.; Batchelor-McAuley, C.; Chen, L.; Compton, R. G., Band Electrodes in Sensing Applications: Response Characteristics and Band Fabrication Methods. *ACS Sens* **2019,** *4* (9), 2250-2266.

30. Heinze, J., Ultramicroelectrodes in Electrochemistry. *Angew. Chem. Int. Ed.* **1993,** *32* (9), 1268-1288.

31. Banks, C. E.; Compton, R. G., Exploring the electrocatalytic sites of carbon nanotubes for NADH detection: an edge plane pyrolytic graphite electrode study. *Analyst* **2005,** *130* (9), 1232-1239.

32. Heller, I.; Kong, J.; Heering, H. A.; Williams, K. A.; Lemay, S. G.; Dekker, C., Individual Single-Walled Carbon Nanotubes as Nanoelectrodes for Electrochemistry. *Nano Lett.* **2005,** *5* (1), 137-142.

33. Maroto, A.; Balasubramanian, K.; Burghard, M.; Kern, K., Functionalized Metallic Carbon Nanotube Devices for pH Sensing. *ChemPhysChem* **2007,** *8* (2), 220-223.

34. Pizzocchero, F.; Gammelgaard, L.; Jessen, B. S.; Caridad, J. M.; Wang, L.; Hone, J.; Boggild, P.; Booth, T. J., The hot pick-up technique for batch assembly of van der Waals heterostructures. *Nat. Commun.* **2016,** *7* (1), 11894.

35. Cao, B.; Grass, T.; Gazzano, O.; Patel, K. A.; Hu, J.; Müller, M.; Huber-Loyola, T.; Anzi, L.; Watanabe, K.; Taniguchi, T.; Newell, D. B.; Gullans, M.; Sordan, R.; Hafezi, M.; Solomon, G. S., Chiral Transport of Hot Carriers in Graphene in the Quantum Hall Regime. *ACS Nano* **2022,** *16* (11), 18200-18209.

36. Aoki, K., Theory of ultramicroelectrodes. *Electroanal.* **1993,** *5* (8), 627-639.

37. Swinya, D. L.; Martín-Yerga, D.; Walker, M.; Unwin, P. R., Surface Nanostructure Effects on Dopamine Adsorption and Electrochemistry on Glassy Carbon Electrodes. *J. Phys. Chem. C* **2022,** *126* (31), 13399-13408.

38. Bath, B. D.; Michael, D. J.; Trafton, B. J.; Joseph, J. D.; Runnels, P. L.; Wightman, R. M., Subsecond adsorption and desorption of dopamine at carbon-fiber microelectrodes. *Anal. Chem.* **2000,** *72* (24), 5994-6002.

39. Hu, K.; Wang, D.; Zhou, M.; Bae, J. H.; Yu, Y.; Xin, H.; Mirkin, M. V., Ultrasensitive Detection of Dopamine with Carbon Nanopipets. *Anal. Chem.* **2019,** *91* (20), 12935-12941.

40. Patel, A. N.; Tan, S. Y.; Miller, T. S.; Macpherson, J. V.; Unwin, P. R., Comparison and reappraisal of carbon electrodes for the voltammetric detection of dopamine. *Anal. Chem.* **2013,** *85* (24), 11755-64.

41. Shang, N. G.; Papakonstantinou, P.; McMullan, M.; Chu, M.; Stamboulis, A.; Potenza, A.; Dhesi, S. S.; Marchetto, H., Catalyst-Free Efficient Growth, Orientation and Biosensing Properties of Multilayer Graphene Nanoflake Films with Sharp Edge Planes. *Adv. Funct. Mater.* **2008,** *18* (21), 3506-3514.

42. Jacobs, C. B.; Vickrey, T. L.; Venton, B. J., Functional groups modulate the sensitivity and electron transfer kinetics of neurochemicals at carbon nanotube modified microelectrodes. *Analyst* **2011,** *136* (17), 3557-3565.

43. Howell, J. O.; Wightman, R. M., Ultrafast voltammetry and voltammetry in highly resistive solutions with microvoltammetric electrodes. *Anal. Chem.* **1984,** *56* (3), 524-529.

44. Compton, R. G.; Banks, C. E., *Understanding Voltammetry*. Imperial College Press: 2010.

45. Velicky, M.; Hu, S.; Woods, C. R.; Toth, P. S.; Zolyomi, V.; Geim, A. K.; Abruna, H. D.; Novoselov, K. S.; Dryfe, R. A. W., Electron Tunneling through Boron Nitride Confirms Marcus-Hush Theory Predictions for Ultramicroelectrodes. *ACS Nano* **2020,** *14* (1), 993-1002.

46. Britnell, L.; Gorbachev, R. V.; Jalil, R.; Belle, B. D.; Schedin, F.; Katsnelson, M. I.; Eaves, L.; Morozov, S. V.; Mayorov, A. S.; Peres, N. M.; Neto, A. H.; Leist, J.; Geim, A. K.; Ponomarenko, L. A.; Novoselov, K. S., Electron tunneling through ultrathin boron nitride crystalline barriers. *Nano Lett.* **2012,** *12* (3), 1707-10.

47. Samuelsson, M.; Armgarth, M.; Nylander, C., Microstep electrodes: band ultramicroelectrodes fabricated by photolithography and reactive ion etching. *Anal. Chem.* **1991,** *63* (9), 931-936.

48. Deakin, M. R.; Wightman, R. M.; Amatore, C. A., Electrochemical kinetics at microelectrodes: Part II. Cyclic voltammetry at band electrodes. *J. Electroanal. Chem. Interf. Electrochem.* **1986,** *215* (1), 49-61.

49. Roberts, J. G.; Sombers, L. A., Fast-Scan Cyclic Voltammetry: Chemical Sensing in the Brain and Beyond. *Anal. Chem.* **2018,** *90* (1), 490-504.

50. Puthongkham, P.; Venton, B. J., Recent advances in fast-scan cyclic voltammetry. *Analyst* **2020,** *145* (4), 1087-1102.

51. Cao, Q.; Puthongkham, P.; Venton, B. J., Review: New insights into optimizing chemical and 3D surface structures of carbon electrodes for neurotransmitter detection. *Anal. Meth.* **2019,** *11* (3), 247-261.

52. Venton, B. J.; Cao, Q., Fundamentals of fast-scan cyclic voltammetry for dopamine detection. *Analyst* **2020,** *145* (4), 1158-1168.

53. Asrat, T. M.; Cho, W.; Liu, F. A.; Shapiro, S. M.; Bracht, J. R.; Zestos, A. G., Direct Detection of DNA and RNA on Carbon Fiber Microelectrodes Using Fast-Scan Cyclic Voltammetry. *ACS Omega* **2021,** *6* (10), 6571-6581.

54. Shin, M.; Copeland, J. M.; Venton, B. J., Real-Time Measurement of Stimulated Dopamine Release in Compartments of the Adult Drosophila melanogaster Mushroom Body. *Anal. Chem.* **2020,** *92* (21), 14398-14407.

55. Hashemi, P.; Dankoski, E. C.; Petrovic, J.; Keithley, R. B.; Wightman, R. M., Voltammetric detection of 5-hydroxytryptamine release in the rat brain. *Anal. Chem.* **2009,** *81* (22), 9462-71.

56. Rodeberg, N. T.; Sandberg, S. G.; Johnson, J. A.; Phillips, P. E.; Wightman, R. M., Hitchhiker's Guide to Voltammetry: Acute and Chronic Electrodes for in Vivo Fast-Scan Cyclic Voltammetry. *ACS Chem Neurosci* **2017,** *8* (2), 221-234.

57. Cryan, M. T.; Ross, A. E., Scalene Waveform for Codetection of Guanosine and Adenosine Using Fast-Scan Cyclic Voltammetry. *Anal. Chem.* **2019,** *91* (9), 5987-5993.

58. Kile, B. M.; Walsh, P. L.; McElligott, Z. A.; Bucher, E. S.; Guillot, T. S.; Salahpour, A.; Caron, M. G.; Wightman, R. M., Optimizing the Temporal Resolution of Fast-Scan Cyclic Voltammetry. *ACS Chem Neurosci* **2012,** *3* (4), 285-292.

59. Lim, G. N.; Ross, A. E., Purine Functional Group Type and Placement Modulate the Interaction with Carbon-Fiber Microelectrodes. *ACS Sens* **2019,** *4* (2), 479-487.

60. Mendoza, A.; Asrat, T.; Liu, F.; Wonnenberg, P.; Zestos, A. G., Carbon Nanotube Yarn Microelectrodes Promote High Temporal Measurements of Serotonin Using Fast Scan Cyclic Voltammetry. *Sensors (Basel)* **2020,** *20* (4), 1173.

61. Ciszkowska, M.; Stojek, Z., Voltammetric and amperometric detection without added electrolyte. *Anal. Chem.* **2000,** *72* (23), 754A-760A.

62. Bond, A. M.; Fleischmann, M.; Robinson, J., Electrochemistry in organic solvents without supporting electrolyte using platinum microelectrodes. *J. Electroanal. Chem. Interf. Electrochem.* **1984,** *168* (1), 299-312.

63. Pletcher, D.; Sotiropoulos, S., Cathodic reduction of oxygen in water and media of low ionic strength. *J. Chem. Soc., Faraday Trans.* **1995,** *91* (3), 457-462.

64. Aoki, K. J.; Chen, J., Insight of electrolyte-free voltammetry at microelectrodes. *Curr. Opin. Electrochem.* **2018,** *10*, 67-71.

65. Chen, Q.; McKelvey, K.; Edwards, M. A.; White, H. S., Redox Cycling in Nanogap Electrochemical Cells. The Role of Electrostatics in Determining the Cell Response. *J. Phys. Chem. C* **2016,** *120* (31), 17251-17260.

66. White, H. S.; McKelvey, K., Redox cycling in nanogap electrochemical cells. *Curr. Opin. Electrochem.* **2018,** *7*, 48-53.

67. Jaworski, A.; Donten, M.; Stojek, Z., Chronoamperometry and pulse voltammetry of uncharged species at microelectrodes in the presence of a very low amount of supporting electrolyte. *Anal. Chim. Acta* **1995,** *305* (1), 106-113.

68. Ciszkowska, M.; Stojek, Z., Voltammetry in solutions of low ionic strength. Electrochemical and analytical aspects. *J. Electroanal. Chem.* **1999,** *466* (2), 129-143.

69. Li, X.; Batchelor-McAuley, C.; Laborda, E.; Compton, R. G., Aqueous Voltammetry in the Near Absence of Electrolyte. *Chem. Eur. J.* **2017,** *23* (60), 15222-15226.

70. Pendley, B. D.; Abruna, H. D.; Norton, J. D.; Benson, W. E.; White, H. S., Analysis of voltammetric half-wave potentials in low ionic strength solutions and voltammetric measurement of ion impurity concentrations. *Anal. Chem.* **1991,** *63* (23), 2766-2771.

71. Oldham, K. B., Theory of microelectrode voltammetry with little electrolyte. *J. Electroanal. Chem. Interf. Electrochem.* **1988,** *250* (1), 1-21.

72. Amatore, C.; Thouin, L.; Fatima Bento, M., Steady state voltammetry at low electrolyte/reactant concentration ratios: what it means and what it does not mean. *J. Electroanal. Chem.* **1999,** *463* (1), 45-52.

73. Cooper, J. B.; Bond, A. M., Microelectrode studies in the absence of deliberately added supporting electrolyte: solvent dependence for a neutral and singly charged species. *J. Electroanal. Chem. Interf. Electrochem.* **1991,** *315* (1), 143-160.

74. Amatore, C.; Oleinick, A. I.; Svir, I. B., Simulation of the double hemicylinder generator–collector assembly through conformal mapping technique. *J. Electroanal. Chem.* **2003,** *553*, 49-61.

75. Wolfrum, B.; Katelhon, E.; Yakushenko, A.; Krause, K. J.; Adly, N.; Huske, M.; Rinklin, P., Nanoscale Electrochemical Sensor Arrays: Redox Cycling Amplification in Dual-Electrode Systems. *Acc. Chem. Res.* **2016,** *49* (9), 2031-40.

76. Wolfrum, B.; Zevenbergen, M.; Lemay, S., Nanofluidic redox cycling amplification for the selective detection of catechol. *Anal. Chem.* **2008,** *80* (4), 972-7.

77. Amatore, C.; Fosset, B.; Maness, K. M.; Wightman, R. M., Theory of electrochemical luminescence at double band electrodes. An examination of "steady-state" diffusion at ultramicroelectrodes. *Anal. Chem.* **2002,** *65* (17), 2311-2316.

78. Rajantie, H.; Strutwolf, J.; Williams, D. E., Theory and practice of electrochemical titrations with dual microband electrodes. *J. Electroanal. Chem.* **2001,** *500* (1-2), 108-120.

79. Barnes, E. O.; Lewis, G. E. M.; Dale, S. E. C.; Marken, F.; Compton, R. G., Generator-collector double electrode systems: A review. *Analyst* **2012,** *137* (5), 1068-1081.

80. Ma, C.; Xu, W.; Wichert, W. R. A.; Bohn, P. W., Ion Accumulation and Migration Effects on Redox Cycling in Nanopore Electrode Arrays at Low Ionic Strength. *ACS Nano* **2016,** *10* (3), 3658-3664.

81. Ciszkowska, M.; Stojek, Z., Analytical application of submicroelectrodes in solutions containing little or no supporting electrolyte. *J. Electroanal. Chem. Interf. Electrochem.* **1986,** *213* (2), 189-201.

82. Belding, S. R.; Limon-Petersen, J. G.; Dickinson, E. J. F.; Compton, R. G., Cyclic Voltammetry in the Absence of Excess Supporting Electrolyte Offers Extra Kinetic and Mechanistic Insights: Comproportionation of Anthraquinone and the Anthraquinone Dianion in Acetonitrile. *Angew. Chem. Int. Ed.* **2010,** *49* (48), 9242-9245.

TOC Graphic (For Table of Contents Only)